Bull Volcanol (2012) 74:1865–1879
DOI 10.1007/s00445-012-0642-9

RESEARCH ARTICLE

Compositional gradients surrounding spherulites in obsidian and their relationship to spherulite growth and lava cooling

James E. Gardner · Kenneth S. Befus · James Watkins · Marc Hesse · Nathan Miller

Received: 28 February 2012 / Accepted: 30 June 2012 / Published online: 24 July 2012

Abstract Spherical masses of crystal fibers (spherulites) crystalize from rhyolitic melt/glass mainly in response to significant undercooling while lava cools. Spherulite growth should induce compositional gradients in the surrounding glass from expulsion of incompatible constituents and diffusion of those constituents away from the spherulite. Finite-difference numerical modeling of one-dimensional diffusion, in which diffusivities are allowed to vary with temperature, is used to investigate how compositional gradients reflect spherulite growth and lava cooling. Overall, three forms of gradients are identified. Elements that diffuse quickly are expelled from the spherulite but then migrate away too quickly to become enriched at the boundary of the spherulite. Elements that diffuse slowly are trapped within the growing spherulite. Between those endmembers are elements that are not trapped, yet diffuse slow enough that they become enriched at the contact. Their slow diffusion away then elevates their concentrations in the surrounding glass. How enriched those elements are at the spherulite-matrix interface and how far their enrichments extend outwards into the glass reflect how spherulites grow and thermal conditions during growth. Concentrations of H_2O, Rb, F, Li, Cl, Na, K, Sr, Cs, Ba, and Be were measured in and around spherulites in obsidian from a 4.7 ± 1 km^3 rhyolite lava dome erupted from Tequila volcano, Mexico. Measurable concentration gradients are found for H_2O, Rb, and F. Attributes of those gradients and the behaviors of the other elements are in accord with their experimentally constrained diffusivities. Spherulites appear to have grown following radial, rather than volumetric, growth. The observed gradients (and lack of others) are more consistent with growth mainly below the glass transition, which would necessitate the dome cooling at ca. 10^{-5} to 10^{-7} °C s^{-1}. Such slow cooling is consistent with the relatively large volume of the dome.

Keywords Obsidian · Spherulite · Tequila volcano · Diffusion · Crystallization

Editorial responsibility: G. Giordano

J. E. Gardner (✉) · K. S. Befus · M. Hesse · N. Miller
Department of Geological Sciences,
Jackson School of Geosciences, The University of Texas at Austin,
Austin, TX 78712-0254, USA
e-mail: gardner@mail.utexas.edu

J. Watkins
Department of Earth and Planetary Sciences,
University of California,
Berkeley, CA, USA

Introduction

Obsidian domes, flows, and pyroclasts are common in the geologic record, yet few have been emplaced in modern times (Johnson and Smith 1974; Singer et al. 2008; Castro and Dingwell 2009). Constraints on the physical processes and timing of mechanisms responsible for obsidian formation are thus derived mostly from textural and structural studies. For example, orientations of bubbles and microlites are used to infer obsidian flow dynamics (Manga 1998; Rust et al. 2003). Flow bands, tuffisite veins, and healed fractures provide field evidence of repeated fragmentation and annealing in volcanic conduits (Tuffen et al. 2003; Gonnermann and Manga 2005; Cabrera et al. 2011).

To fully interpret lava textures and structures, the thermal history of lava needs to be understood and in particular that history where the features occur. To constrain how cooling varied with time at specific locations within lava, the thermal record needs to be preserved. One such record may be preserved as the relaxation temperature of glass, which preserves the cooling history across the glass transition (T_g) (Gottsmann and Dingwell 2001). Compositional

gradients surrounding spherulites could also preserve a record of the thermal history, with the idea that because spherulites may grow over a range in temperature, the compositional record preserved around them might yield information on the conditions under which they formed (e.g., Lofgren 1971a; Fenn 1977; Swanson 1977; Castro et al. 2008; Watkins et al. 2009). Specifically, incompatible constituents are expelled into the surrounding rhyolitic melt/glass glass as the spherulite grows (e.g., Kesler and Weiblen 1968). Those constituents then diffuse away from the enriched boundary into the surrounding matrix forming compositional gradients (Castro et al. 2008; Watkins et al. 2009). The attributes of those gradients (how enriched the boundary is; how far away constituents migrate) could be a proxy for thermal conditions during growth, because diffusion rates vary with temperature (e.g., Zhang et al. 2010).

Recent reviews of spherulites are given in Castro et al. (2008), Watkins et al. (2009), and Seaman et al. (2009). In general, spherulites are spherical aggregates of crystals (Fig. 1) that radiate outwards from a central point (Lofgren 1971a; MacArthur et al. 1998). The fact that natural spherulites occur almost exclusively in glass requires conditions in which crystal nucleation is suppressed (Swanson 1977; Fenn 1977). When they do nucleate, experimental evidence indicates that silica and feldspar polymorphs grow in acicular or fibrous crystal morphologies because of large undercooling (Kirkpatrick 1975; Swanson 1977; Fenn 1977). Where spherulites occur naturally it is common for them to reach millimeters to centimeters in size, but in rare instances can be a meter or more (Carmichael et al. 1974; Davis and McPhie 1996; MacArthur et al. 1998; Smith et al. 2001; Castro et al. 2008; Watkins et al. 2009; Seaman et al. 2009). In this paper, we focus on spherulites thought to have grown during cooling. Such spherulites typically overprint microlite flow banding in obsidian, but often flow bands are deformed around the spherulites (Stevenson et al. 1994; Monecke et al. 2004; Tuffen and Castro 2009) and the coarseness of the spherulite appears to require relatively hot conditions to grow (e.g., Swanson et al. 1989). Those observations argue for growth both above and below T_g, which for dry rhyolite is 600–700 °C (Dingwell 1998; Gottsmann et al. 2002).

Spherulite growth involves diffusion and uptake of compatible elements into the crystallizing region, as well as rejection and expulsion of incompatible elements from the crystallizing region (Kesler and Weiblen 1968; Castro et al. 2008; Watkins et al. 2009). The details of that process are complicated, and depend on the composition and morphology of crystallizing phases, which in turn, are a complex function of melt composition, temperature, pressure, and degree of undercooling (Kirkpatrick 1975). In general, partitioning of elements between fibrous crystals and the melt or glass phase takes place at the tips of fibers as well as along fibers as they grow laterally. As crystal fibers impinge upon one another, incompatible elements may become trapped in the interstitial regions of melt or glass within the spherulite. The extent of incompatible element expulsion thus depends on crystal growth rate as well as the rate at which elements diffuse away from crystallizing regions. Both of those factors depend on temperature, and by extension, the cooling history of the obsidian host.

Previous studies show that water gradients surrounding spherulites can be modeled using the advection-diffusion equation (Castro et al. 2008; Watkins et al. 2009). Those studies held temperature constant, however, and so they could not establish the thermal histories recorded by those gradients. Here, we build on those models by incorporating the temperature dependence of diffusion to predict the attributes of compositional gradients of water and other constituents around spherulites. An important issue is that compositional gradients will reflect not only cooling but also how the spherulite grew. In this study, therefore, we investigate the dependence of compositional gradients on various growth laws for spherulites as well as their dependence on cooling rate. Newly acquired compositional data for water and other trace elements surrounding spherulites are presented for comparison to model predictions and to constrain the likely thermal conditions and spherulite growth behavior during cooling of obsidian lava.

Numerical model

In our model for spherulite growth, we treat the spherulite as a single, isolated phase that is spherically symmetric. As the spherulite grows outward, incompatible elements are concentrated at the spherulite-melt or spherulite-glass boundary and diffuse outward into the surrounding matrix. The concentration distribution of incompatible elements around the spherulite is governed by the growth rate and the element-specific diffusivity. To simulate this phenomenon, we use finite-difference numerical modeling to solve for one-dimensional diffusion:

$$\left(\frac{\partial C}{\partial t}\right)_i = \frac{1}{x^2}\frac{\partial}{\partial x}\left(D_i x^2 \left(\frac{\partial C}{\partial x}\right)_i\right) \quad (1)$$

where $\left(\frac{\partial C}{\partial t}\right)_i$ is the change in concentration of constituent i with time t, $\left(\frac{\partial C}{\partial x}\right)_i$ is the change in concentration of i with distance x from the spherulite boundary in the matrix, and D_i is diffusivity of i. We represent the motion of the spherulite-matrix boundary with an inflow condition that simulates the incompatible constituent

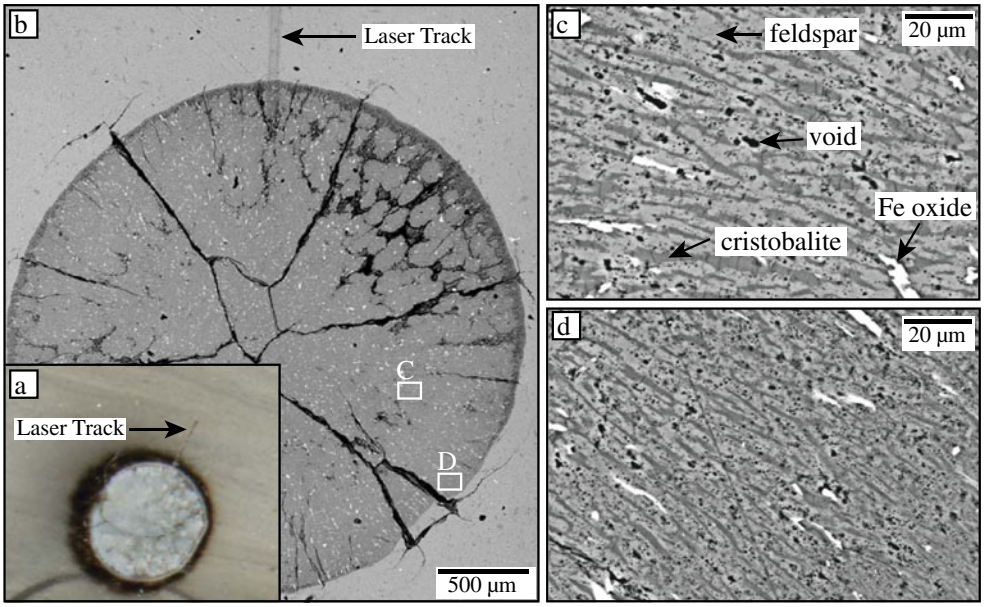

Fig. 1 **a** Photomicrograph of spherulite in surrounding glass (see (**b**) for scale), with laser track indicated. The *dark halo* probably reflects oxidation of the glass (Castro et al. 2009); **b** SEM image of that same spherulite, with the same laser track indicated. Positions of (**c**) and (**d**) are shown; **c** SEM close-up of the interior of the spherulite, with feldspar (*light gray*), cristobalite (*dark gray*), Fe oxide (*bright*), and vesicles (*black*) indicated; **d** SEM close-up near the rim, with the same phases as in (**c**)

expelled into the matrix. That inflow is controlled by our choice of growth law, a parameter we treat as an unknown (see below). With each increment of growth, a discrete amount of i is expelled into the spherulite-matrix boundary. The concentration of i at the spherulite-matrix boundary changes with time as a function of input by the spherulite growth rate and reduction via diffusion. The model is governed by two boundary conditions. The first conserves mass during diffusion and incremental growth using a conservative discretization that ensures that diffusive fluxes entering and leaving each cell are equal (LeVeque 2002). The second condition fixes the concentration of i to a set value in the far-field matrix (which is assumed homogeneous).

As mentioned earlier, some incompatible elements may not be fully expelled. We do not distinguish between specific mechanisms of incompatible element trapping, but instead account for incomplete expulsion by specifying that only part of the mass of i is expelled into the spherulite-matrix boundary during an increment of growth.

In many respects our model is similar to those of Castro et al. (2008) and Watkins et al. (2009), except that we allow D_i (in square micrometers per second) to vary with temperature, such that

$$D_i = D_o \exp\left(\frac{-E_A}{RT}\right) \quad (2)$$

where D_o is a constant, E_A is activation energy, R is the gas constant, and T is temperature (in degrees Celsius). Diffusivities are calculated iteratively for each step in time, using values for D_o and E_A provided by Zhang et al. (2010). Water diffusivity is known to vary with both temperature and dissolved water content, and so we vary D_{H_2O} with both using the model of Ni and Zhang (2008). For comparison purposes we refer to D_i values at 500 °C (i.e., D_i^{500}). Values of D_i^{500} in dry rhyolite range mainly from $\leq 10^{-8}$ to $\geq 10^{1}$ μm^2 s^{-1} (Fig. 2).

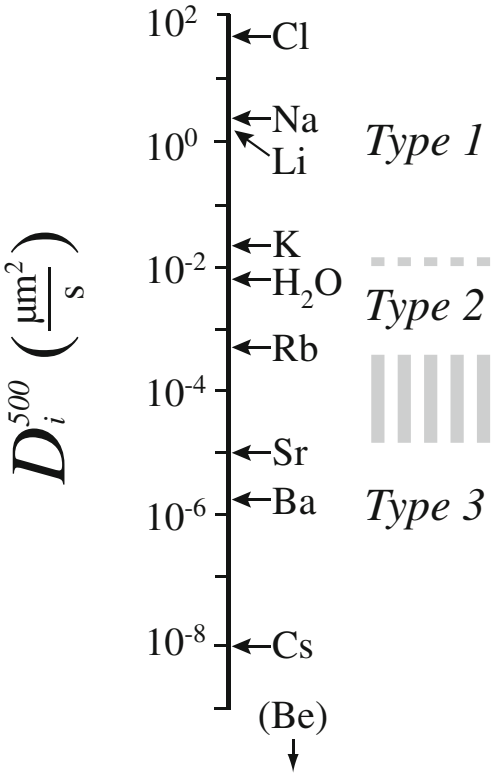

Fig. 2 Representative elements arranged vertically according to their diffusivities in dry rhyolite at 500 °C (D_i^{500}), as estimated from Zhang et al. (2010). Water diffusivity corresponds to melt water content of 0.12 wt.% (Ni and Zhang 2008). Compositional gradients displayed by those elements around three Tequila spherulites and the approximate transitions between gradients are marked

Cooling model for obsidian lava

In this section, we obtain a temperature–time history that potential represents the environment in which spherulites form. This serves as a starting point for investigating the impact of growth laws on compositional gradients around spherulites. Manley (1992) numerically modeled the cooling of ca. 50-m thick obsidian lava, based on the 0.1 km^3 Obsidian Dome (Fig. 3a). Spherulites in a glassy matrix are found in Obsidian Dome at heights of ca. 10–35 m above the base of the flow. At a height of 30 m, the numerical model predicts that temperature dropped from emplacement temperature (~900 °C) to ~740 °C in the first ten years, to ~400 °C in 30 years, and 200 °C in ~60 years (Fig. 3a). We approximate that thermal history with an exponential decay in temperature with time (t) in the form

$$T = T_o \exp(-(at)^n) \tag{3}$$

where T_o is initial or emplacement temperature, and a and n are fit parameters, which we set at $a = 1\times10^{-9}$ °C s^{-1} and $n = 1.5$ (Fig. 3b). A closer fit to the results of Manley (1992) could be found if either a or n were allowed to vary with time, but we only seek a first-order approximation for cooling, and thus keep them constant.

Equation 3 is used below to evaluate how compositional gradients change with growth law for a specific cooling history. Once those effects are established, we evaluate the impact of different cooling histories. We neglect the release of latent heat from spherulite crystallization, assuming that such heat is removed faster than spherulites grow (Watkins et al. 2009). Latent heat release could be incorporated into the cooling model.

Growth laws for spherulites

Watkins et al. (2009) assumed that spherulite growth is modulated by enrichment of water in the surrounding glass, with growth slowing as the boundary becomes more enriched (Frank 1950; Keith and Padden 1963, 1964). Castro et al. (2008) used a growth rate that slows exponentially with time, justified by the assumption that growth is limited by diffusion. Here, we assume that spherulite growth is controlled by temperature. That assumption is justified because diffusion of compatible constituents slows as temperature decreases (Eq. 2).

We assume that spherulite growth can be described as either radial or volumetric. In the case of radial growth, each step of growth expels mass as a proportion of its radius. Growth rate is either held constant or allowed to slow linearly or exponentially as temperature drops (Eqs. 4, 5, and 6):

$$\left(\frac{dr}{dt}\right) = \left(\frac{dr}{dt}\right)_n \quad \text{(radial, constant)} \tag{4}$$

$$\left(\frac{dr}{dt}\right) = \left(\frac{dr}{dt}\right)_n - \left(\frac{dr}{dt}\right)_n \frac{(T - T_n)}{(T_f - T_n)} \quad \text{(radial, linearly decreasing)} \tag{5}$$

$$\left(\frac{dr}{dt}\right) = \left(\frac{dr}{dt}\right)_n \exp(-c(T_n - T)) \quad \text{(radial, exponentially decreasing)} \tag{6}$$

where $\left(\frac{dr}{dt}\right)$ and T are radial growth rate (in micrometers per hour) and temperature at time t, $\left(\frac{dr}{dt}\right)_n$ and T_n are radial growth rate (in micrometers per hour) and nucleation temperature, T_f is final temperature, and c is a fit parameter. Both forms of slowing radial growth converge to similar rates at low temperatures, but the exponential growth law (Eq. 6) decreases more quickly.

In the case of volumetric growth, each step expels mass in proportion to volume. Growth rate is either held constant or decreases exponentially with T (Eqs. 7 and 8):

$$\left(\frac{dV}{dt}\right) = \left(\frac{dV}{dt}\right)_n \quad \text{(volumetric, constant)} \tag{7}$$

$$\left(\frac{dV}{dt}\right) = \left(\frac{dV}{dt}\right)_n \exp(-c(T_n - T)) \quad \text{(volumetric, exponentially decreasing)} \tag{8}$$

where $\left(\frac{dV}{dt}\right)$ is volumetric growth rate (in cubic micrometers per hour) at time t and $\left(\frac{dV}{dt}\right)_n$ is volumetric growth rate at nucleation. Both forms of volumetric growth correspond to slowing radial growth, because the width of each newly added annulus shortens with time.

Below, all model results are derived by assuming T_o = 800 °C and growth ceases at 400 °C (T_f). Unless stated otherwise $\left(\frac{dr}{dt}\right)_n$ at 700 °C is set equal to 0.25 μm h^{-1} or its equivalent volumetric rate. For nucleation at other temperatures $\left(\frac{dr}{dt}\right)_n$ is calculated from the growth law assuming $\left(\frac{dr}{dt}\right)_n = 0.25\ \mu m\ h^{-1}$ at 700 °C. In the case of constant rate laws, however, the growth rate at nucleation is set at 0.25 μm h^{-1} (or its volumetric equivalent) regardless of T_n. Because growth rates depend on T, how big a spherulite gets partly depends on T_n (Fig. 4). Finally, except where stated, half of the total mass of an element is expelled into the melt/glass in each increment of growth.

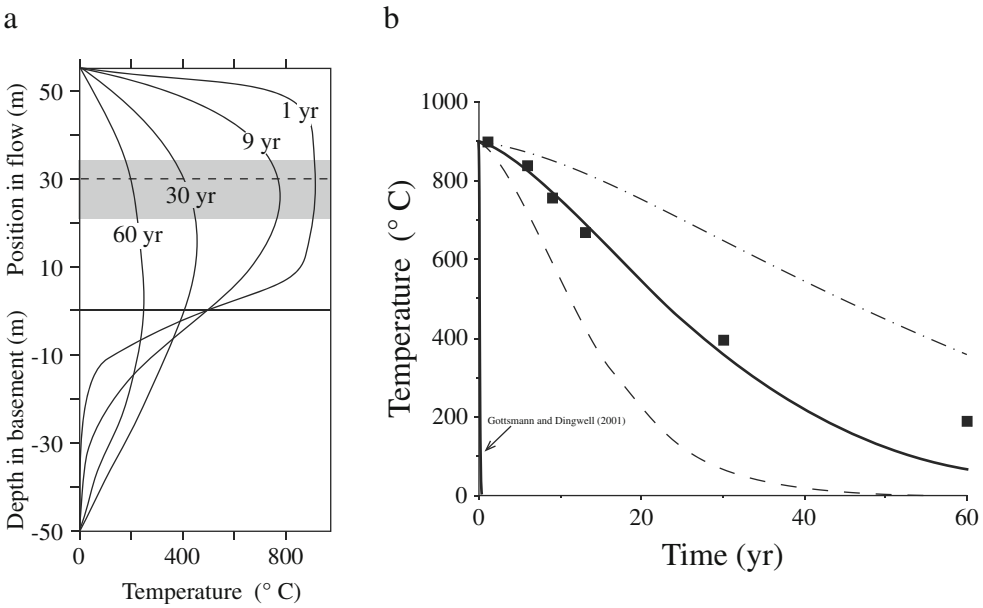

Fig. 3 **a** Cooling of Obsidian Dome, modified from Manley (1992). Curves show temperature distributions at various times (in years) after emplacement. *Shaded region* shows depths in the flow where spherulites are found. **b** Thermal history (*solid curve*) calculated using Eq. 3, setting $a=1\times10^{-9}$ °C s^{-1} and $n=1.5$. *Squares* are temperatures at 30 m from the bottom of Obsidian Dome (*dashed line* in (**a**)). *Dashed curve* is for $a=2\times10^{-9}$ °C s^{-1} and *dotted–dashed* curve for 5×10^{-10} °C s^{-1}; $n=1.5$ for both. The evolution of temperature based on the cooling rate from Gottsmann and Dingwell (2001) is shown for reference

Compositional gradients surrounding spherulites

To establish what compositional gradients are expected to surround spherulites, we solved Eq. 1 for a range of diffusivities. Our modeling, in conjunction with results of Keith and Padden (1963), identifies that compositional gradients should generally take on one of three forms (Fig. 5). First, there are constituents that are expelled but diffuse so quickly away from the boundary that they do not become enriched; we refer to those as Type 1 gradients (Fig. 5a). At the other extreme, Keith and Padden (1963) showed that constituents that diffuse very slowly relative to spherulite growth are trapped within the spherulite. In that case, there is no change in concentration between the spherulite and matrix (Type 3 gradients; Fig. 5b). In between, there are constituents that escape (at least partially) the spherulite, but their diffusion is sluggish enough that they remain enriched at the interface (Type 2 gradients; Fig. 5c). Their concentrations decrease away from the spherulite as they diffuse away. Water contents have been observed to form Type 2 gradients (Castro et al. 2008; Watkins et al. 2009).

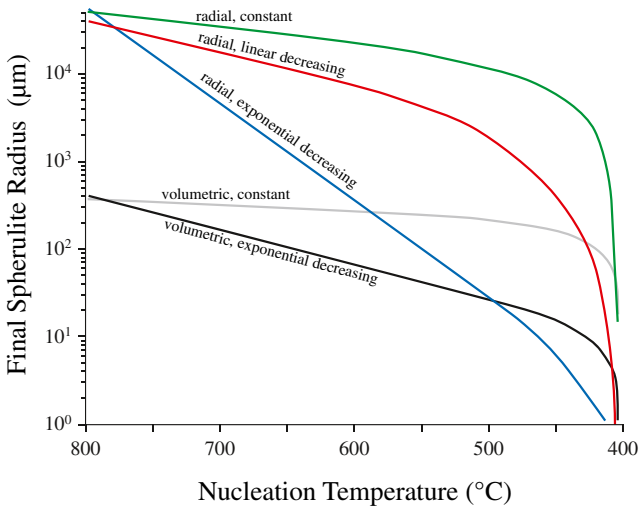

Fig. 4 Spherulite size (in micrometers) as a function of nucleation temperature (T_n). Curves correspond to various growth laws: constant radial growth (*green curve*; Eq. 4), linearly decreasing radial growth (*red*; Eq. 5), exponentially decreasing radial growth (*blue*; Eq. 6), constant volumetric growth (*gray*; Eq. 7), and exponentially decreasing volumetric growth (*black*; Eq. 8). All curves derived by setting T_o= 800 °C and T_f=400 °C. For non-constant growth laws $\left(\frac{dr}{dt}\right)_n$ was set at 0.25 μm h^{-1} at T_n=700 °C and then varied with T according to growth law. Growth rate for constant growth is 0.25 μm h^{-1} or its volumetric equivalent

The transitions between gradient types occur at relatively faster diffusivities for radial growth laws than for volumetric growth laws (Fig. 6). For example, constant radial growth leads to Type 2 gradients for elements with $D_i^{500}\leq10^0$ μm s^{-1}, whereas exponentially slowing volumetric growth results in such gradients only for elements with $D_i^{500}\leq10^{-4}$ μm s^{-1}. Transitions shown in Fig. 6 result from setting T_n=650 °C and $\left(\frac{dr}{dt}\right)_n = 0.25$ μm s^{-1}. If spherulites nucleate at hotter temperatures or if $\left(\frac{dr}{dt}\right)_n$ <0.25 μm s^{-1} then the transitions shift to lower values of D_i^{500}. If the spherulites continue growing below 400 °C, then the transitions shift to higher values of D_i^{500}.

Type 2 gradients can be described by how enriched the boundary layer is and how far a gradient extends into the surrounding matrix (Fig. 5d). The enrichment at the interface (equal to the ratio of the interface concentration to that in the far-field glass) reflects a competition

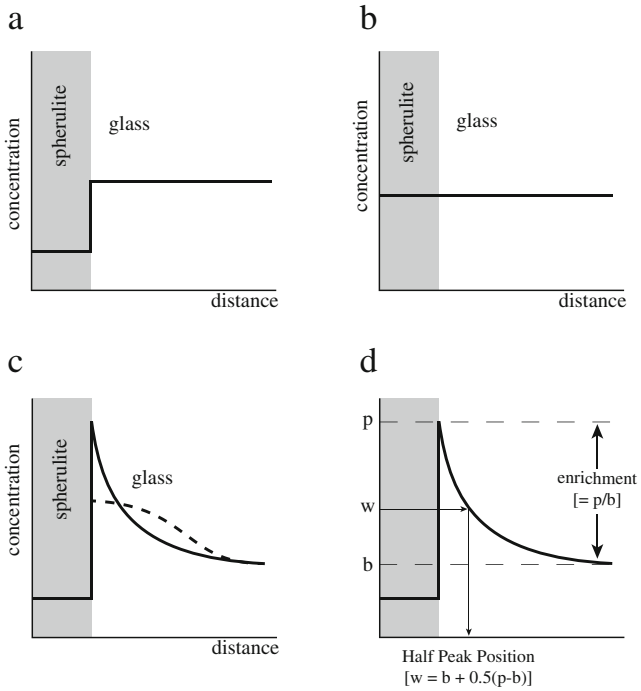

Fig. 5 Schematic drawings of compositional gradient types expected to occur around spherulites. **a** Type 1 gradients consist of relatively low concentrations in the spherulite but constant concentrations in the surrounding glass. **b** Type 3 gradients consist of unchanging concentrations across the spherulite-glass interface. **c** Type 2 gradients consist of relatively depleted contents in the spherulite and convex downward variations in contents in the surrounding glass. The dotted curve shows a relaxed Type 2 gradient, which results when diffusion continues after spherulite growth ceases. **d** Type 2 gradients can be described by the enrichment at the interface and its "half-peak" position

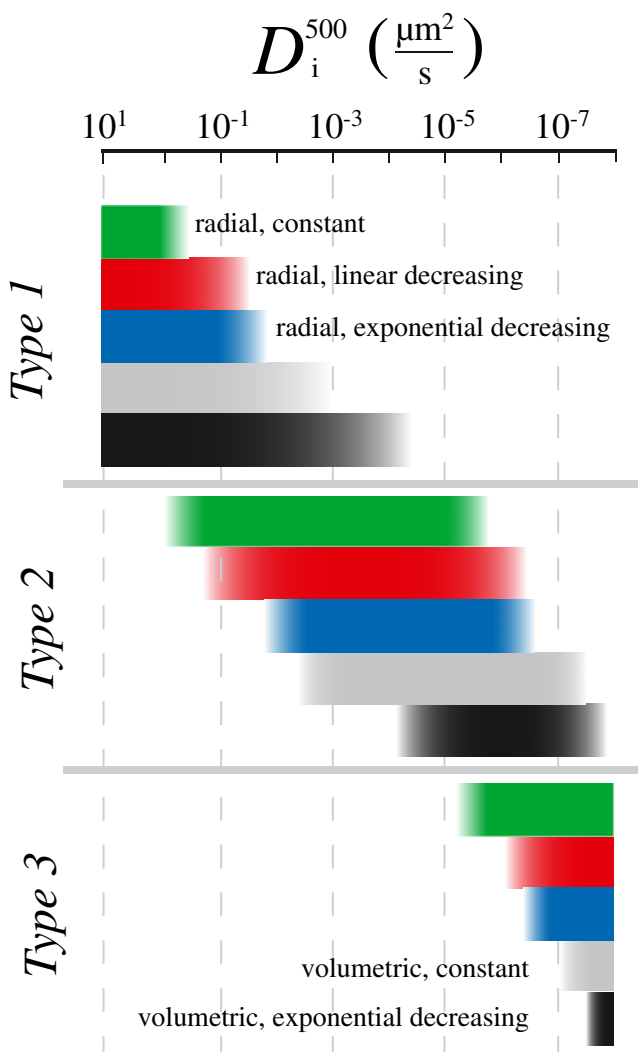

Fig. 6 Ranges in diffusivities that result in the three different types of compositional gradients, using the various growth laws (Eqs. 4, 5, 6, 7, and 8). All results calculated for T_n=650 °C with $\left(\frac{dr}{dt}\right)_n = 0.25\ \mu m\ h^{-1}$. Colors match those in Fig. 4

between expulsion and diffusion. For a given diffusivity, growth law plays an important role in enrichment (Fig. 7). Radial growth results in enrichments that increase with spherulite size. The degree of enrichment also depends on the relationship between growth rate and temperature. Constant radial growth rate (Eq. 4) results in greater enrichments than do radial growth rates that decrease with temperature (Eqs. 5 and 6). In contrast to radial growth, volumetric growth results in enrichments that decrease with spherulite size (Fig. 7). The lower degree of enrichment around larger spherulites results from a rapid decrease in growth rate at higher temperatures while diffusion is still fast. Regardless of growth law, enrichments would be greater if spherulites continue growing below 400 °C because of slowing diffusion.

A second characteristic of Type 2 gradients is how far they extend into the matrix (Fig. 5d). Establishing that distance in natural data could be difficult, however, because it requires finding precisely where the concentration of an element exceeds that of its glass concentration. We thus instead focus on the position along a gradient where the concentration equals the average between the peak and background concentrations. Such "Half-Peak" positions are controlled mainly by D_i, with faster diffusing elements migrating farther away in a given amount of time. Half-Peak position also varies with growth law (Fig. 8). In the case of radial growth, that position increases as enrichment increases, but extends relatively farther away if growth slows. In contrast, volumetric growth results in shorter Half-Peak positions that decrease as enrichment increases.

Regardless of growth law, Type 2 behavior is expected for diffusivities that range by several orders of magnitude (Fig. 6). Such gradients should thus exist for some constituents under almost all circumstances. How enriched those

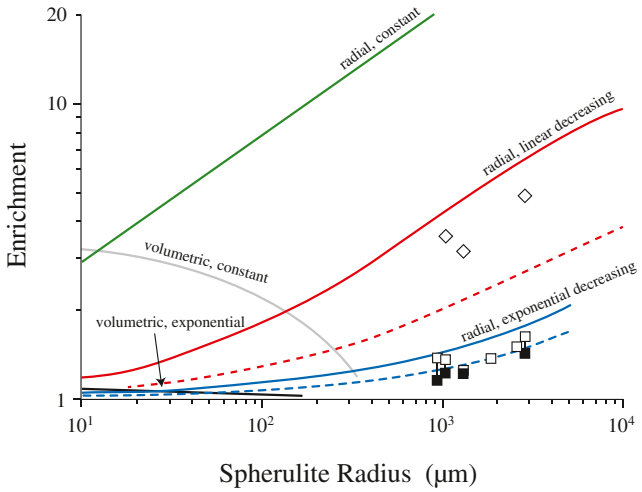

Fig. 7 Variations in enrichment as a function of final spherulite size for the various growth laws; the range in size was produced by varying T_n. All curves (labeled and colored as in Fig. 4) were derived by setting T_o=800 °C and T_f=400 °C. In addition, growth rates at nucleation for non-constant growth laws were set at 0.25 μm h^{-1} at T_n=700 °C and then varied with T according to growth law. *Solid curves* are for Rb diffusivity ($D_{Rb}^{500} = 10^{-3.3}$ μm^2 s^{-1}); *dashed curves* are for D_{H_2O}. *Diamonds* are Rb enrichments around spherulites in Tequila obsidian; *squares* are water enrichments around those and other Tequila spherulites, defined by either the greatest concentration at the rim (*open squares*) or the highest concentration in the longer, broader gradient outside of steep gradients next to the rims (*filled squares*)

gradients are reflects growth, and so examining enrichments surrounding spherulites of different sizes should help distinguish how spherulites grow.

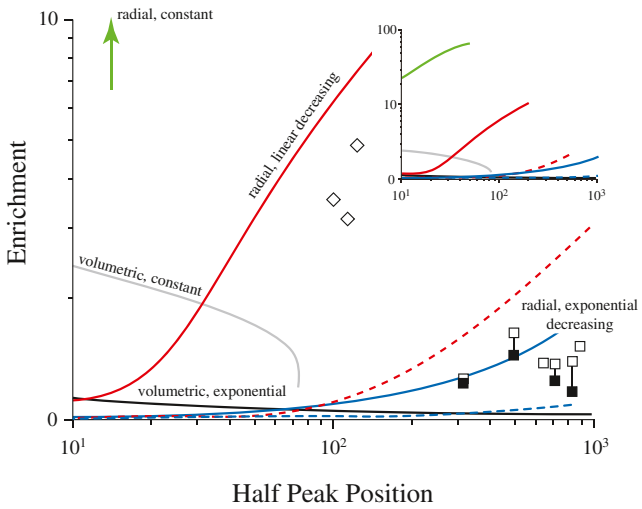

Fig. 8 Variations in enrichment as a function of Half Peak position for the various growth laws; the range in size was produced by varying T_n. All curves (labeled and colored as in Fig. 4) were derived using the same assumptions as those in Fig. 7. *Insert* shows larger scale for enrichment to include constant radial growth. Enrichments of Rb (*diamonds*) and water (*squares*) around spherulites in Tequila obsidian are shown (see Fig. 7 for details)

Impact of cooling rate on compositional gradients

Equation 3 with our preferred values for a and n was used to derive the forms of compositional gradients that should surround spherulites. That model predicts cooling of ~$10^{-6.2}$ °C s^{-1} (Fig. 3). Using differential scanning calorimetry, Gottsmann and Dingwell (2001) estimated that the Rosse Roche obsidian lava cooled at ~$10^{-3.2}$ °C s^{-1} or three orders of magnitude faster than specified in our model (Fig. 3). At that rate, the time allowed for spherulites to grow would be much shorter, resulting in far less time for diffusion.

To investigate the full impact of cooling rate on the form of Type 2 gradients, we modeled the behavior of an element with $D_i^{500} = 10^{-3.3}$ (Fig. 9). Nucleation temperature (T_n) was fixed at 650 °C, but $\left(\frac{dr}{dt}\right)_n$ was varied in order to produce spherulites of different sizes. We modeled spherulite growth at constant radial rates (Eq. 4) and exponentially decreasing volumetric rates (Eq. 8), because those result in the most disparate spherulite growth (Fig. 4). As an intermediate example, spherulites were also modeled with a linearly decreasing radial rate (Eq. 5). We find that the Half Peak position normalized to Enrichment varies greatly depending on cooling rate, growth law, and growth rate (Fig. 9). For all growth behaviors, faster cooling results in smaller ratios related to spherulites of any given size. In fact, given the diffusivity assumed, Half-Peak positions will not extend further than 10–15 times Enrichment if cooling rate exceeds 10^{-4} °C s^{-1}. In many cases, a given initial growth rate results in similar normalized Half-Peak positions around spherulites of substantially different sizes. For example, Half-Peak positions will be on order of ten times that of enrichment away from 100-μm to 10-cm spherulites, if they all start growing radially at ~0.1 μm h^{-1} and that rate decreased linearly (Fig. 9b). Only when growth rate slows rapidly does the normalized Half-Peak position depend significantly on initial growth rate (Fig. 9a).

Compositional gradients expected around spherulites thus depend greatly on how quickly obsidian lava cools (Fig. 9). For spherulites of similar size, the Half-Peak position relative to Enrichment will extend much further if lava cools slowly, similar to the model of Manley (1992), then if it cools quickly, like that measured by Gottsmann and Dingwell (2001). The clear distinction between cooling rates indicates that compositional gradients can indeed preserve a record of the cooling of lava.

Spherulites from Tequila volcano, Mexico

An important prediction from our modeling is that various types of compositional gradients should surround any given spherulite. To explore that, we analyzed spherulites from an obsidian lava erupted from Tequila Volcano, Mexico, the

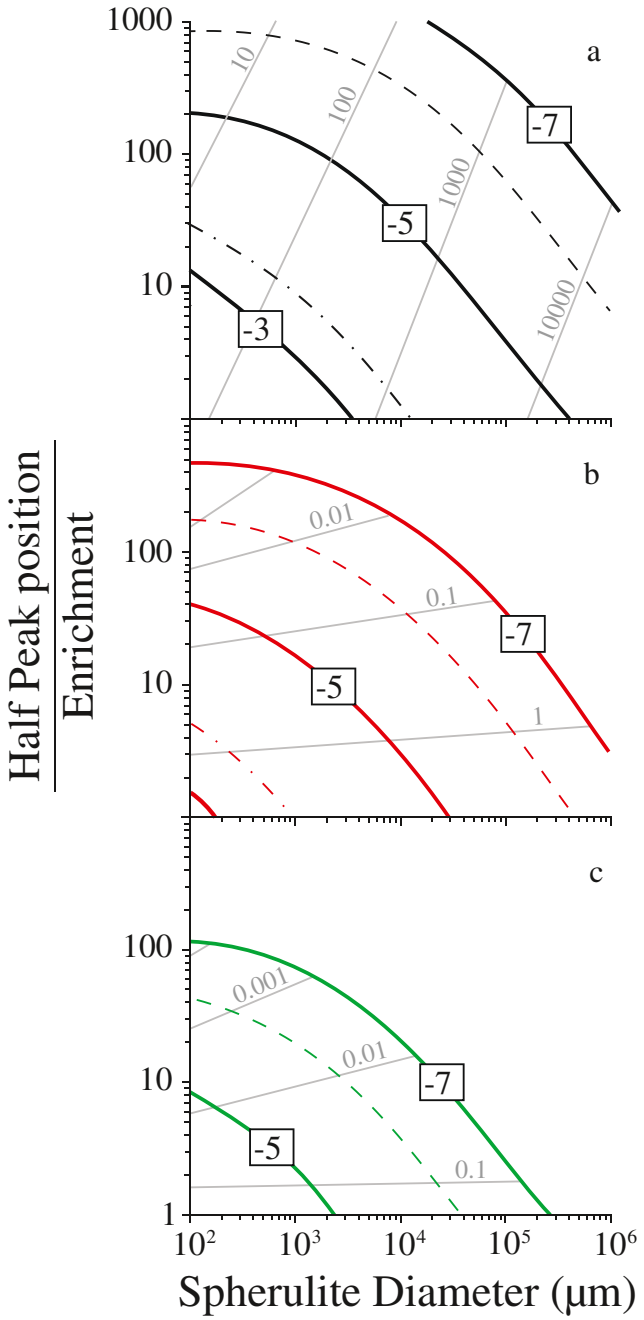

Fig. 9 The ratio of Half Peak position to Enrichment as a function of final size of spherulites grown at **a** an exponentially decreasing volumetric rate (Eq. 8), **b** a linearly decreasing radial rate (Eq. 5), or **c** a constant linear rate (Eq. 4) (colors match those in Fig. 4). *Solid curves* are for cooling rates labeled in $\log_{10}$ units (°C s^{-1}); *dashed curve* is for cooling rate from Eq. 3 using preferred values for *a* and *n*; *dotted–dashed curve* is for cooling using measured rate of Gottsmann and Dingwell (2001). *Gray lines* connect results for given nucleation growth rates (in micrometers per hour). All results set T_o=800 °C, T_f=400 °C, T_n=650 °C, and $D_{Rb}^{500} = 10^{-3.3}$ μm^2 s^{-1}

same one in which Watkins et al. (2009) measured water concentrations surrounding other spherulites. The sample came from the northern margin of an obsidian lava dome with a volume of 4.7±1 km^3, which erupted 642 ± 6 ka (sample TEQ-18 in Lewis-Kenedi et al. 2005). The non-porphyritic lava is rhyolitic, with high-silica rhyolitic glass (Table 1). The glass contains subtle flow bands of varying amounts of microlites of feldspar and minor amounts of Fe oxides and pyroxene. Feldspar microlites are generally tabular in shape and range in size from 10×2 to 100×20 μm. Fe oxides are typically equant in shape and generally 5 μm in size. Trace pyroxenes are generally 10×2 μm in size.

Here, we measured water concentrations in traverses away from six spherulites, not analyzed by Watkins et al. (2009), and then for other elements in traverses from three of those six (Fig. 1). We targeted mainly elements for which values for D_i are constrained by experimental data in water-poor rhyolite at temperatures similar to those assumed in our model. Water contents were measured using synchrotron FTIR; concentrations of Na, K, Li, Rb, Sr, Ba, Cs, and Be were measured by laser ablation (LA)-ICP-MS; Cl and F concentrations were measured by electron microprobe (see Appendix for methods).

The spherulites are 2 to 6.5 mm in diameter; four are spherical in shape, the other two are more ellipsoidal. The three targeted for LA-ICP-MS analyses are 2.3, 2.9, and 6.5 mm. Of those three, Cl and F concentrations were measured away from the smallest and largest. All six spherulites consist of anorthoclase ($Ab_{75\pm1}Or_{24\pm1}An_{1\pm1}$) and cristobalite (Watkins et al. 2009), with minor Fe oxides and less than a few percent vesicular glass (Fig. 1). The average sizes of the five largest feldspar and cristobalite are relatively constant across the spherulites, except in the outer ~50 μm, where they decrease in size to less than 1 μm (Fig. 10). Those outer ~50 μm also appear more vesicular. Little difference exists in grain size between spherulites,

Table 1 Compositions of whole rock and matrix glass of tequila obsidian lava

	Whole rock	Matrix glass
SiO_2	74.1	75.00
TiO_2	0.11	0.20
Al_2O_3	12.3	13.58
FeO*	1.35	1.28
MnO	0.05	0.00
MgO	0.08	0.10
CaO	0.42	0.39
Na_2O	4.35	4.53
K_2O	4.62	4.92

Whole-rock analysis (TEQ-18) is from Lewis-Kenedi et al. (2005). Matrix glass is the average composition (*n*=5) analyzed by electron microprobe (normalized to 100 %), with all Fe reported as FeO; oxides are in weight percent

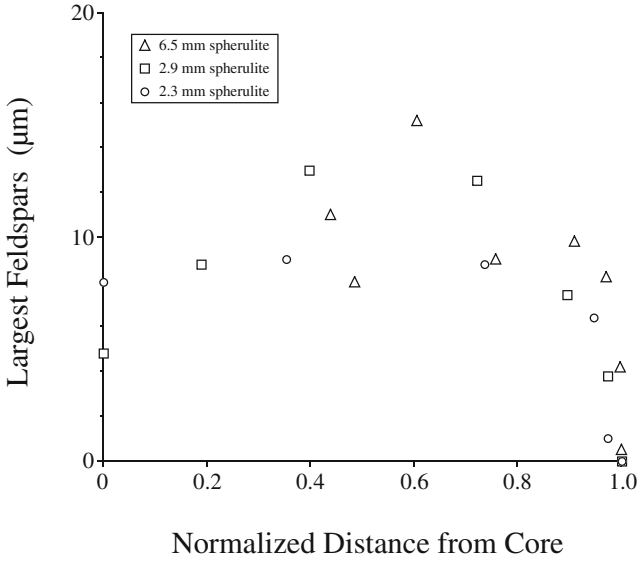

Fig. 10 Grain size variations inside of spherulites. Sizes are averages of the five largest feldspars at a given position; cristobalite shows the same variations in size with distance. *Symbols* represent three spherulites: *circles* for the 2.3-mm spherulite, *squares* for the 2.9-mm spherulite, and *triangles* for 6.5 mm spherulite. Positions have been normalized to the full radius of the spherulite to show the same relative positions in the spherulites

except the core of one of the small spherulites is slightly finer grained than the other.

Water concentrations are 0.14 to 0.18 wt.% at the rims of the six spherulites, and decrease to ~0.11 wt.% at about 1,600–1,800 μm away (Fig 11a). The very low water concentrations in the glass argue that the sample has not been hydrated, and therefore the spherulites did not grow at low temperature via fluid fluxing (Lofgren 1971b). The greatest water concentration is found at the rim of the largest spherulite. Next to the rims of four of the six spherulites, water gradients in the first 100–150 μm of glass are steeper than the more extensive gradients that extend outward from ~150 μm. Watkins et al. (2009) found similarly steep enrichments around other spherulites in the sample. Interestingly, they also found relative depletions in water near the rims of others. Water concentrations were not analyzed in the interiors of the spherulites but are expected to be low (Watkins et al. 2009). Water concentrations thus form Type 2 gradients.

Compositional gradients similar to those of water were found for Rb (Fig. 11b) and F (Fig. 11c). Rb in the glasses reaches peaks of ~450 to 575 parts per million (ppm) next to spherulite rims, and decreases to ~150±30 ppm ~600–700 μm away. We cannot accurately quantify Rb in the spherulites, because we do not know their bulk compositions, but if we assume that they have similar silica contents as the glass, the average concentration of Rb is ~20–80 ppm, significantly less than in the glass. Fluorine is 1,600–1,900 ppm in glasses at spherulite rims, which is significantly more than the ~1,100 ppm in glasses far away (Fig. 11c).

Lithium is depleted in the spherulites relative to the glasses (Fig. 12). In the glasses, however, Li contents are essentially homogeneous. Li thus appears to form Type 1 gradients, such that it was expelled from the spherulites but diffused away too quickly to become measurably enriched. We note that Li is one of fastest diffusing elements in dry rhyolite at temperatures of interest (Jambon and Semet 1978). Potassium shows similar distributions as Li, with lower concentrations in the spherulite, but no enrichment at the rims (Fig. 12). K thus appears to form Type 1 gradients. Likewise, Cl concentrations are constant in the glass (Fig. 12). We did not measure Cl in the spherulites, but it should be in low abundance. Cl diffuses even faster than Li (Jambon and Semet 1978; Bai and Koster van Groos 1994), and so in fact the two should behave similarly. Sodium follows a similar trend as Li, Cl, and K, except that it is relatively enriched in the spherulite. Greater Na/K ratios in the spherulites relative to those in the glass are consistent with the sodic-rich feldspar in the spherulites. Although Na appears to have been compatible, and hence cannot strictly follow our model, its lack of depletion at spherulite rims indicates that Na diffusion was fast relative to spherulite growth, which is essentially Type 1 behavior. Na diffusivity in dry rhyolite is in fact almost as fast as Li (Margaritz and Hofmann 1978; Jambon and Semet 1978; Watson 1981; Jambon 1982). Therefore, Li, Na, Cl, and K all formed Type 1 gradients. Of those, K has the lowest diffusivity (Jambon and Carron 1976; Jambon 1982).

Concentrations of Ba, Sr, Cs, and Be are relatively constant from inside the spherulite to the glass outside (Fig. 13). Ba and Sr concentrations correlate with each other, suggesting that their occasional fluctuations represent feldspar microlites in the glass. Sr and Ba may or may not have been incompatible in the spherulite, but Cs and Be were most likely highly incompatible, and so at least those elements should have been enriched in the surrounding glass. None, however, show differences between spherulite and glass, and so it appears that all form Type 3 gradients. In fact, all four diffuse orders of magnitude slower than water, although Be diffusivity is known only at high temperatures (Margaritz and Hofmann 1978; Jambon 1982; Baker 1992; Mungall et al. 1999).

Three groups of elements have been identified. One group (Li, K, Na, and Cl) forms Type 1 compositional gradients, the second (H_2O, Rb, and F) forms Type 2 gradients, and the third (Ba, Sr, Cs, and Be) forms Type 3 gradients. Overall, the groupings are consistent with experimentally calibrated diffusivities (Fig. 2). All of those that form Type 1 gradients diffuse faster than H_2O, and all of

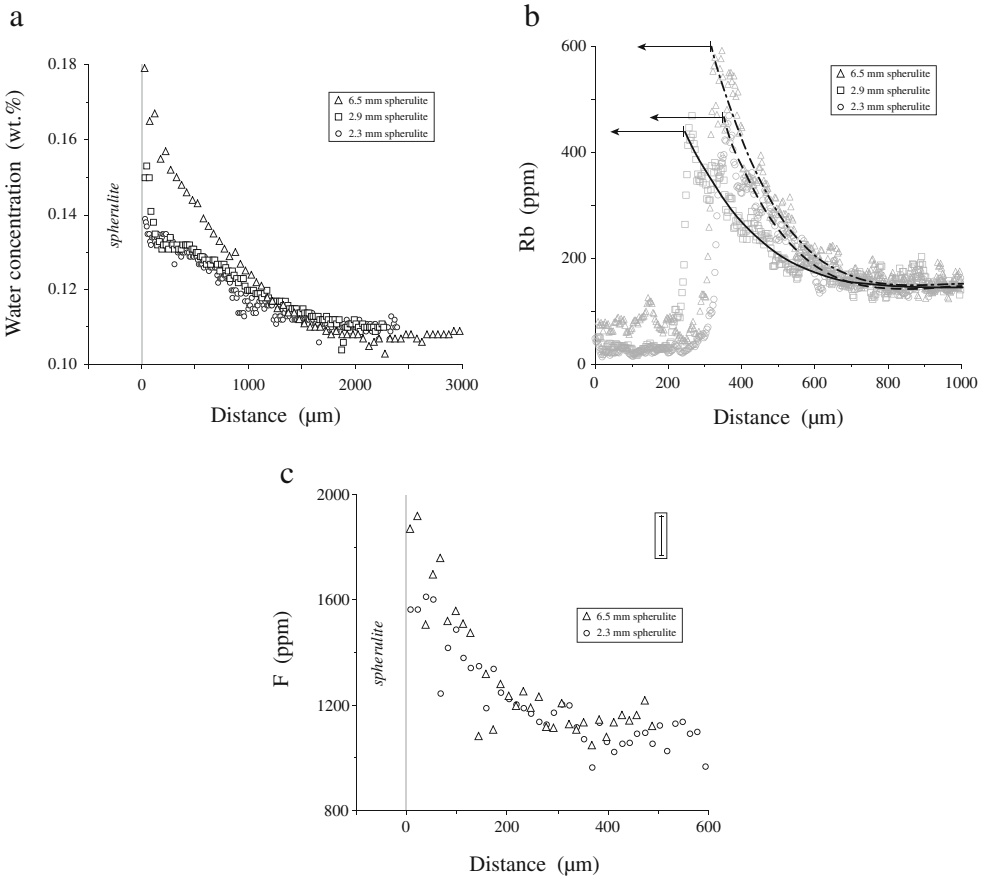

Fig. 11 Compositional gradients measured for **a** water, **b** Rb, and **c** F. *Curves* for Rb are best fits to 5-point running averages of data, with r^2 values of >0.92; *solid line* for *squares*; *dashed line* for *circles*; *dotted–dashed* line for *triangles* (see Fig. 10 for symbols). Water and fluorine contents were measured in the glass only; the average error on F analyses is shown. Rb was measured in continuous traverses starting in the spherulites and moving outward into the glass; the approximate positions of the spherulite-glass interfaces are marked for each profile

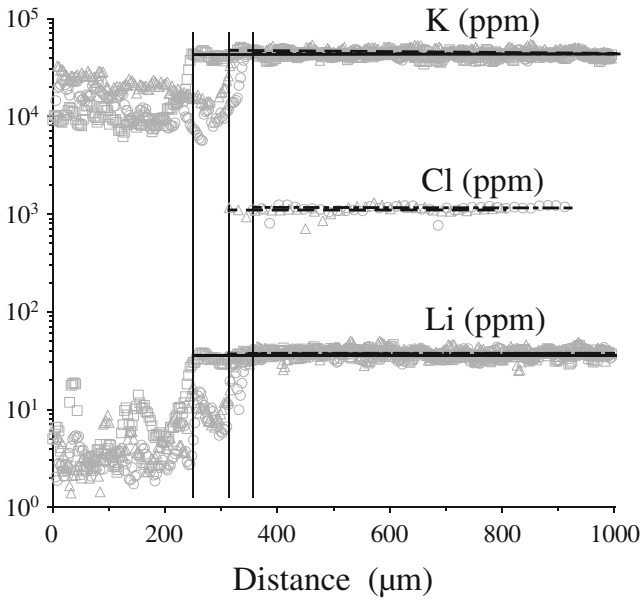

Fig. 12 Compositional gradients measured for K, Cl, and Li (see Fig. 10 for *symbols* and Fig. 11 for *lines*). Approximate positions of the spherulite-glass interfaces are marked. Note the lack of any enrichment in the glass at the interface

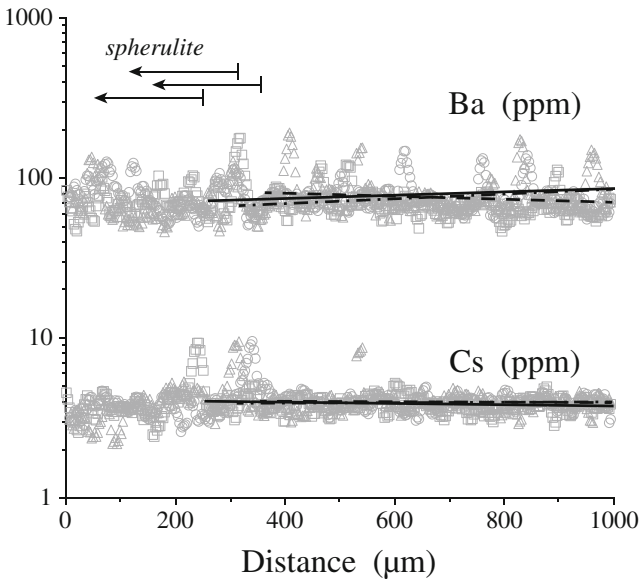

Fig. 13 Compositional gradients measured for Ba and Cs (see Fig. 10 for *symbols* and Fig. 11 for *lines*). Approximate positions of the spherulite-glass interfaces are marked. Oscillations in Ba contents probably result from analyses of feldspar microlites in the glass

those that form Type 3 gradients diffuse slower than Rb. In regards to H_2O and Rb, Half Peak positions for water are at ~450–650 μm, whereas those for Rb are at ~75–100 μm. Greater distances are expected for faster diffusing elements, and indeed water diffuses faster than Rb (Jambon 1982; Ni and Zhang 2008). The consistent groupings of elements and the extents of Type 2 gradients thus indicate that our model correctly predicts elemental behavior during spherulite growth.

Fluorine formed well-defined compositional gradients similar to those of water and Rb (Fig. 11c). Half-Peak positions for F occur at ~30–45 μm, much closer than those for Rb or water (Fig. 11). Such distances suggest that D_F^{500} should be much lower than $D_{H_2O}^{500}$ and only slightly lower than D_{Rb}^{500}. Unfortunately, we cannot confirm that because D_F in dry rhyolite at temperatures of interest is unknown (Baker and Balcone-Boissard 2009). Fluorine diffusivity in phonolite ($D_F^{500} = 10^{-3.6}$ to $10^{-4.8}$ μm^2 s^{-1}; Zhang et al. 2010) and in aluminosilicate melts ($10^{-6.2}$) (Dingwell and Scarfe 1985) is slower than D_{Rb}^{500} (Fig. 2). The relative positions of D_{Rb}^{500} and D_{Sr}^{500} in Fig. 2 suggest that F diffusivity in dry rhyolite may be similar to that in phonolite.

Enrichments in H_2O and Rb generally increase as spherulite size increases (Fig. 7). That is true for water, whether enrichment is defined using either the steep gradients next to the rims or the longer, broader profiles outside of the steep gradients (Fig. 11a). For each spherulite, Rb is more enriched relative to water, which is consistent with the lower diffusivity of Rb. Greater enrichments at the rims of larger spherulites indicate that their growth can be described as some form of radial growth, and not volumetric (Fig. 7).

The compositional gradients in H_2O and Rb associated with spherulites of different size can be modeled following our assumptions in Fig. 9, focusing on radial growth laws (Fig. 14). If growth were constant, then the spherulites grew, on average, at ~$10^{-2.5}$ μm h^{-1} while the lava cooled at ~$10^{-6.8}$ °C s^{-1}. If radial growth slowed while the lava cooled, then the spherulites started growing at ~10^{-1} to ~10^{0} μm h^{-1} while the lava cooled at ~$10^{-4.9}$ to $10^{-5.9}$ °C s^{-1}. Although we cannot identify a preferred radial growth law from our dataset, we note that crystals are often found to experimentally grow at relatively constant rates (e.g., Fenn 1977; Swanson 1977; Baker and Freda 2001).

Growth and cooling rates in Fig. 14 were derived assuming that spherulites grew between 650 (T_n) and 400 °C (T_f), which approximates growth occurring at T_g and below (Dingwell 1998; Gottsmann et al. 2002). Alternatively, growth can be assumed to occur only above T_g, such that T_f =650 °C. We model the latter case using only constant radial growth (Eq. 4) because the times allowed for growth above T_g are short. Compositional gradients similar to those observed for Rb can be produced for spherulites of 2.3 to 6.5 mm in diameter by changing T_n from 651° to 780 °C as cooling rate increases from $10^{-6.5}$ to $10^{-4.5}$ °C s^{-1}. Nucleation must occur at higher temperatures at faster cooling rates in order to allow enough time to make appropriately sized spherulites. At those conditions growth rates are ~1.4 to 2.4 μm h^{-1}, with the larger spherulite inferred to grow

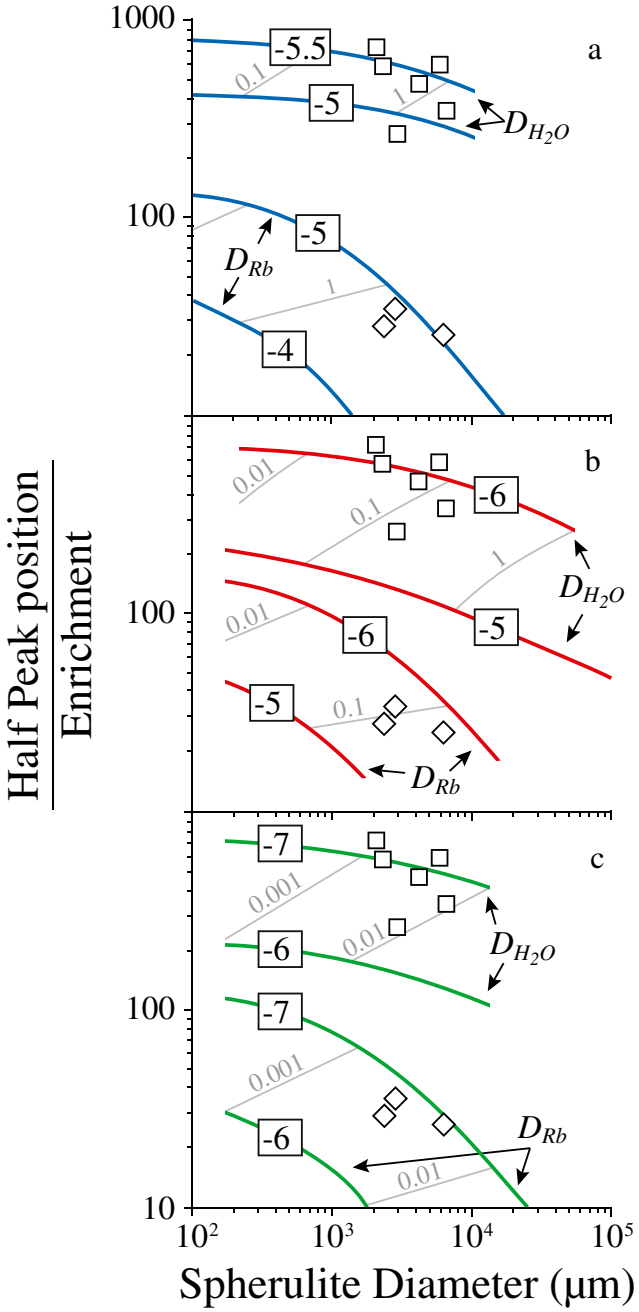

Fig. 14 The ratio of Half Peak position to Enrichment as a function of size of spherulites grown radially at **a** an exponentially decreasing rate (Eq. 6), **b** a linearly decreasing rate (Eq. 5), or **c** a constant rate (Eq. 4). Two sets of curves are shown in each, labeled in $\log_{10}$ units (°C s^{-1}) according to the diffusivity used (see Fig. 9 for other details). *Diamonds* and *squares* are for Rb and water data, respectively, around Tequila spherulites

faster than the small ones, in order to generate the greater enrichment of Rb at its boundary (Fig. 11b). Those same conditions cannot, however, produce water gradients similar to those observed. Instead, higher values of T_n (up to ~100 °C hotter) and slower growth rates (up to ten times slower) are needed to approximate the observed water gradients. Regardless of conditions, growth at temperatures above T_g causes elements with significantly lower diffusivities than Rb to display Type 2 behavior. In particular, Sr and Ba should form Type 2 gradients. In addition, the more rapid growth at hotter conditions should result in Type 2 gradients displayed elements with higher diffusivities than water, such as K (but not Li or Cl).

The model for growth above T_g assumed that both growth and diffusion cease at T_g (set at 650 °C). In reality, elements would continue to diffuse as the glass cools. Post-growth diffusion changes the shape of the concentration profiles; in particular, the steep enrichments of Type 2 gradients relax (Fig. 5c). Such relaxation lowers concentrations near the spherulite boundary and moves mass outwards, producing a more gentle decrease in concentration. Some water gradients around spherulites in our Tequila sample appear partially relaxed (Watkins et al. 2009), but many others are not (e.g., Fig. 11a). Castro et al. (2008) also found both relaxed and unrelaxed gradients for water. For both Rb and F, the broad plateaus of relaxed concentrations should extend outward by ca. 50 to 200 μm, depending on cooling rate. Instead, no such relaxation is observed in the Rb or F gradients (Fig. 11b, c). As for Ba and Sr, their diffusivities are low enough that neither move appreciably when temperature is below 650 °C. Thus, the Type 2 gradients that they should form during growth above T_g would be preserved, in contrast to the gradients measured (Fig. 13). Finally, K diffusivity is high enough at temperatures below 650 °C that its Type 2 gradient produced during growth would essentially completely relax, and thus appear as if it behaved as a Type 1 element (Fig. 12).

Overall, the observed compositional gradients for the three sets of elements (Figs. 11, 12, and 13) are consistent with relatively slow growth during slow cooling, if growth occurred mainly below T_g (Fig. 14). Narrow ranges of growth rates and cooling rates reproduce both water and Rb gradients for each growth law, with the closest agreement occurring using constant radial growth (Fig. 14). In contrast, modeled growth above T_g temporarily produces Type 2 gradients for Rb and water (and F), but they would not be fully preserved and instead show pronounced relaxations. Such growth would also result in Type 2 gradients for slower diffusing elements, such as Sr and Ba. Those elements, however, form Type 3 gradients (Fig. 13). Despite the inconsistencies between measured and predicted gradients for growth above T_g, such growth is supported by the vesicular nature of the spherulite interiors (Fig. 1). On the other hand, Lofgren (1971a) showed that crystals in spherulites decrease in size dramatically from ca. 10 to <1 μm when the temperature at which they grow decreases from 700 to below 500 °C. The precipitous decrease in grain size in our spherulites is consistent with growth at relatively cool conditions (Fig. 10). We also note that water gradients surrounding four of the six spherulites are in fact steeper in the first 100–150 μm away from the rims (Fig. 11a). One explanation for such sharp increases is that diffusion slowed substantially during the final stages of growth. Slower water diffusion in that case could only result from cooler temperatures because water diffusivity increases with water content in the melt/glass (Ni and Zhang 2008). It thus appears that the final stages of growth for some spherulites occurred at conditions significantly below T_g.

The evidence is thus equivocal in regards to the timing of spherulite growth, but the observed compositional gradients seem to favor spherulites growing mainly below T_g. If so, such growth could only occur if cooling rates are on order of 10^{-5} to 10^{-7} °C s^{-1} (Fig. 14). Such slow cooling is expected for relatively large volume flows (Manley 1992). Indeed, the lava has an estimated volume of 4.7 ± 1 km^3 (Lewis-Kenedi et al. 2005). It appears that compositional gradients around spherulites may in fact record some aspects of thermal history of lava.

Summary

Finite-difference numerical modeling of one-dimensional diffusion, in which diffusion is allowed to vary with temperature, identified three general forms of compositional gradients that should occur around spherulites in obsidian lava. Fast-diffusing elements are expelled from the spherulite but migrate away fast enough to not become enriched at the spherulite-glass contact. Very sluggish elements get trapped inside the growing spherulite (Keith and Padden 1963). Little difference in their concentrations will exist between spherulite and glass. There are then elements that will not be trapped but diffuse slowly enough that they become enriched at the contact. Their diffusion away from the contact elevates their concentrations in the surrounding glass. How enriched those elements are at the contact and how far their enrichments extend outwards into the glass reflect how spherulites grew, how fast they grew, and under what thermal conditions they grew. Enrichments of water and Rb around spherulites in an obsidian lava dome from Tequila volcano, Mexico, suggest that those spherulites grew radially. Spherulite growth mainly below the glass transition (assumed≈650 °C) at cooling rates of ~10^{-5} to 10^{-7} °C s^{-1} is indicated by attributes of the water and Rb gradients as well as the types of gradients displayed by

slower diffusing elements and variations in grain size inside the spherulites. In contrast, growth mainly above the glass transition at faster cooling rates is indicated by the vesicular nature of the spherulites. Better understanding of the growth mechanism of spherulites would allow one scenario to be favored over the other, which would then allow compositional gradients surrounding spherulites to be used to infer the thermal conditions during their growth.

Acknowledgments This work was partially supported by a grant from the National Science Foundation (EAR-1049829) to J.E.G. and analytical fee support from the Jackson School of Geosciences to K.S.B. Critical reviews by Dr. Hugh Tuffen and an anonymous reviewer greatly improved the manuscript.

Appendix A: analytical methods

Water concentrations were measured by synchrotron radiation-source Fourier transform infrared spectroscopy (SR-FTIR) at the Advanced Light Source Beamline 1.4.4 using a Thermo Nicolet Nexus 870 FTIR Spectrometer interfaced with a Continuum XL IR microscope. Measurements were made using a 15× Reflachromat objective, MCT detector, and KBr beamsplitter. The spot size for the infrared beam is diffraction limited, about 2–4 μm in this spectral region, and the step size between individual measurements can be as short as 0.1 μm. Transects were oriented perpendicular to spherulite rims and measurements were made on the surrounding glassy matrix. Because the wafers are only ~500-μm thick effects of spherulite curvature were neglected. We collected 32 scans per spot and 128 scans for the background. A new background was collected every 5 minutes during each transect.

Concentrations were determined from FTIR measurements using the Beer–Lambert law

$$C_i = \left(\frac{AM_i}{\rho d \varepsilon_i}\right) 100 \quad \text{(A1)}$$

where M_i is the molecular weight (in grams per mole), A is the absorbance, ρ is the sample density (≈2,300 g/L for rhyolite glass), d is the thickness of the wafer (in centimeters), and ε_i is the molar absorption coefficient (in liters per centimeter per mole). Total water concentrations (H_2O_t) are determined from the 3,570-cm^{-1} peak height using a linear baseline correction (Newman et al. 1986). Total water contents are not high enough to determine the relative abundance of hydrous species (OH) and molecular water (H_2O_m). Because absolute values of water concentration are not important for our analysis, we report the relative uncertainty between spot analyses, which is estimated to be less than 0.01 wt.% based on variability in the glass matrix far from the spherulites.

Trace element concentrations were measured by LA-ICP-MS at the University of Texas at Austin, using a New Wave Research UP 193-FX fast excimer (193 nm wavelength, 4–6 ns pulse width) laser system coupled to an Agilent 7500ce ICP-MS (Table 2). The laser system uses a large format laser cell (232 cc with He carrier gas flow of 200 mL min^{-1}) equipped with a roving collector cup for direct sampling of the ablation plume. Reference standards and rhyolite sections were sampled as line scans (5 μm s^{-1}), using a rectangular 5×50 μm slit aperture oriented with long-axis normal to the scan direction, an energy density (fluence) of 671±18 Jcm^{-2}, and 10 Hz repetition rate. The ICP-MS, operated at an RF power of 1,500 W and Ar carrier flow of 1.1 Lmin^{-1}, monitored masses ^{7}Li, ^{9}Be, ^{23}Na, ^{29}Si, ^{39}K, ^{85}Rb, ^{88}Sr, ^{133}Cs, and ^{137}Ba. Analyte integration times varied between 5 and 100 ms, for a sampling period of

Table 2 Analytical conditions for LA-ICP-MS measurements

	^{7}Li	^{9}Be	^{23}Na	^{39}K	^{85}Rb	^{88}Sr	^{133}Cs	^{137}Ba
Integration times (ms)	30	100	5	5	10	50	100	50
NIST 612/BCR-2G[a]	99	111	102	95	102	102	104	101
NIST 610/BCR-2G[a]	97	108	104	100	100	102	107	106
BCR-2G/NIST 612[a]	103	92	98	105	99	99	96	99
NIST 610/NIST 612[a]	99	98	102	105	99	100	103	105
Primary reference[b]	BCR	BCR	612	BCR	BCR	612	BCR	612
Glass (ppm)[c]	16	3	18,493	13,506	117	4	2	34
Detection limits (ppm)	0.27	22	14.17	15.46	0.15	0.04	0.04	0.47

[a] Secondary standard recoveries (in percent)/primary standard. Recoveries versus those of GeoREM preferred values. See http://georem.mpch-mainz.gwdg.de

[b] Primary reference used for each element. USGS BCR-2G (BCR); NIST 612 (612)

[c] Average of median concentrations for all traverses

0.5462 s; equivalent to a reading every 2.731 μm. Time-resolved intensities were converted to concentration (in parts per million) equivalents using Iolite software (University of Melbourne), with ^{29}Si as the internal standard, and a Si index value of 35.8 wt.%. Baselines were determined from 60 s glass blank intervals measured while the laser was off and all masses were scanned by the quadrupole. USGS BCR-2 G was used as the primary reference standard for all analytes except ^{11}B, ^{88}Sr, and ^{137}Ba, for which NIST 612 was used. Average detection limits for line scans were 14 (Be) to 1305 (Na) times lower than the corresponding median concentrations. Recoveries (relative 1 s deviations versus GeoREM preferred values) among analytes for secondary standards run as unknowns against primary standards were typically better than 3 %. Based on these observations, we conservatively assign 5 % as relative uncertainties.

Major-element compositions and fluorine and chlorine contents of matrix glasses were measured using the JEOL Superprobe electron microprobe at the University of Texas at Austin. Major elements were analyzed using 10 nA beam current, 15 keV accelerating voltage, and a beam defocused to 10 μm size. Spot analyses of F and Cl were made along linear traverses orientated perpendicular to spherulite rims in 15-μm intervals, using a 40-nA beam current, 15 keV accelerating voltage, and a beam defocused to 10 μm size. Both F and Cl were measured on peak for 90 s, and 60 s off-peak for background, using the Durango apatite and a scapolite as standards, respectively.

References

Bai TB, Koster van Groos AF (1994) Diffusion of chlorine in granitic melts. Geochim Cosmochim Acta 58:113–123

Baker DR (1992) Tracer diffusion of network formers and multicomponent diffusion in dacitic and rhyolitic melts. Geochim Cosmochim Acta 56:617–632

Baker DR, Balcone-Boissard H (2009) Halogen diffusion in magmatic systems: our current state of knowledge. Chem Geol 263:82–88

Baker DR, Freda C (2001) Eutectic crystallization in the undercooled orthoclase-quartz-H_2O system: experiments and simulations. Eur J Mineral 13:453–466

Cabrera A, Weinberg RF, Wright HMN, Zlotnik S, Cas RAF (2011) Melt fracturing and healing: a mechanism for degassing and origin of silicic obsidian. Geology 39:67–70

Carmichael I, Turner F, Verhoogen J (1974) Igneous petrology. McGraw-Hill, New York, 739 p. ISBN 0070099871

Castro JM, Dingwell DB (2009) Rapid ascent of rhyolitic magma at Chaiten Volcano, Chile. Nature 461:780–783

Castro JM, Beck P, Tuffen H, Nichols ARL, Dingwell DB, Martin MC (2008) Timescales of spherulite crystallization in obsidian inferred from water concentration profiles. Am Mineral 93:1816–1822

Castro JM, Cottrell E, Tuffen H, Logan AV, Kelley KA (2009) Spherulite crystallization induces Fe-redox redistribution in silicic melt. Chem Geol 268:272–280

Davis B, McPhie J (1996) Spherulites, quench fractures and relict perlite in a Late Devonian rhyolite dyke, Queensland, Australia. J Volcanol Geotherm Res 71:1–11

Dingwell DB (1998) The glass transition in hydrous granitic melts. Phys Earth Planet Int 107:1–8

Dingwell DB, Scarfe CM (1985) Chemical diffusion of fluorine in melts in the system Na_2O–Al_2O_3–SiO_2. Earth Planet Sci Lett 73:377–384

Fenn PM (1977) The nucleation and growth of alkali feldspars from hydrous melts. Can Mineral 15:135–161

Frank FC (1950) Radially symmetric phase growth controlled by diffusion. Proc Roy Soc Lond 201:586–599

Gonnermann HM, Manga M (2005) Flow banding in obsidian: a record of evolving textural heterogeneity during magma deformation. Earth Planet Sci Lett 236:135–147

Gottsmann J, Dingwell DB (2001) The cooling of frontal flow ramps: a calorimetric study on the Rocche Rosse rhyolite flow, Lipari, Aeolian Islands, Italy. Terra Nova 13:157–164

Gottsmann J, Giordano D, Dingwell DB (2002) Predicting shear viscosity during volcanic processes at the glass transition: a calorimetric calibration. Earth Planet Sci Lett 198:417–427

Jambon A (1982) Tracer diffusion in granitic melts: experimental results for Na, Rb, Cs, Ca, Sr, Ba, Ce, Eu to 1300 °C and a model of calculation. J Geophys Res 87:10797–10810

Jambon A, Carron JP (1976) Diffusion of Na, K, Rb and Cs in glasses of albite and orthoclase composition. Geochim Cosmochim Acta 40:897–903

Jambon A, Semet MP (1978) Lithium diffusion in silicate glasses of albite, orthoclase, and obsidian composition: an ion-microprobe determination. Earth Planet Sci Lett 37:445–450

Johnson RW, Smith IE (1974) Volcanoes and rocks of Saint Andrew Strait, Papua new Guinea. J Geol Soc Aust 21:333–351

Keith HD, Padden FJ (1963) A phenomenological theory of spherulitic crystallization. J Appl Phys 34:2409–2421

Keith HD, Padden FJ (1964) Spherulitic crystallization from the Melt. II. Influence of fractionation and impurity segregation on the kinetics of crystallization. J Appl Phys 35:1286–1296

Kesler SE, Weiblen PW (1968) Distribution of elements in a spherulitic andesite. Am Mineral 53:2025–2035

Kirkpatrick R (1975) Crystal growth from the melt: a review. Am Mineral 60:798–814

LeVeque RJ (2002) Finite volume methods for hyperbolic conservation laws. Cambridge University Press, Cambridge, 558 p

Lewis-Kenedi C, Lange R, Hall C, Delgado-Grenados H (2005) The eruptive history of the Tequila volcanic field, western Mexico: ages, volumes, and relative proportions of lava types. Bull Volcanol 67:391–414

Lofgren GE (1971a) Spherulitic textures in glassy and crystalline rocks. J Geophy Res 76:5635–5648

Lofgren GE (1971b) Experimentally produced devitrification textures in natural rhyolitic glass. Geol Soc Am Bull 82:111–124

MacArthur A, Cas R, Orton G (1998) Distribution and significance of crystalline, perlitic and vesicular textures in the Ordovician Garth Tuff (Wales). Bull Volcanol 60:260–285

Magaritz M, Hofmann AW (1978) Diffusion of Sr, Ba and Na in obsidian. Geochim Cosmochim Acta 42:595–605

Manga M (1998) Orientation distribution of microlites in obsidian. J Volcanol Geotherm Res 86:107–115

Manley CR (1992) Extended cooling and viscous flow of large, hot rhyolite lavas: implications of numerical modeling results. J Volcanol Geotherm Res 53:27–46

Monecke T, Renno AD, Herzig PM (2004) Primary clinopyroxene spherulites in basaltic lavas from the Pacific-Antarctic Ridge. J Volcanol Petrol Geotherm 130:51–59

Mungall JE, Dingwell DB, Chaussidon M (1999) Chemical diffusivities of 18 trace elements in granitoid melts. Geochim Cosmochim Acta 63:2599–2610

Newman S, Stolper E, Epstein S (1986) Measurement of water in rhyolitic glasses: calibration of an infrared spectroscopic technique. Am Mineral 71:1527–1541

Ni H, Zhang Y (2008) H_2O diffusion models in rhyolitic melt with new high pressure data. Chem Geol 250:68–78

Rust A, Manga M, Cashman K (2003) Determining flow type, shear rate and shear stress in magmas from bubble shapes and orientations. J Volcanol Geotherm Res 122:111–132

Seaman S, Dyar M, Marinkovic N (2009) The effects of heterogeneity in magma water concentration on the development of flow banding and spherulites in rhyolitic lava. J Volcanol Geotherm Res 183:157–169

Singer BS, Jicha BR, Harper MA, Naranjo JA, Lara LE, Moreno-Roa H (2008) Eruptive history, geochronology, and magmatic evolution of the Puyehue-Cordon Caulle volcanic complex, Chile. Geol Soc Am Bull 120:599–618

Smith RK, Tremallo RL, Lofgren GE (2001) Growth of megaspherulites in a rhyolitic vitrophyre. Am Mineral 86:589–600

Stevenson RJ, Briggs RM, Hodder APW (1994) Physical volcanology and emplacement history of the Ben Lomond rhyolite lava flow, Taupo Volcanic Centre, New Zealand. N Z J Geol Geophys 37:345–358

Swanson SE (1977) Relation of nucleation and crystal-growth rate to the development of granitic textures. Am Mineral 62:966–978

Swanson SE, Naney MT, Westrich HR, Eichelberger JC (1989) Crystallization history of Obsidian Dome, Inyo Domes, California. Bull Volcanol 51:161–176

Tuffen H, Castro JM (2009) The emplacement of an obsidian dyke through this ice: hrafntinnuhryggur, Krafla Iceland. J Volcanol Geotherm Res 185:352–366

Tuffen H, Dingwell DB, Pinkerton H (2003) Repeated fracture and heating of silicic magma generate flow banding and earthquakes? Geology 31:1089–1092

Watkins J, Manga M, Huber C, Martin M (2009) Diffusion-controlled spherulite growth in obsidian inferred from H_2O concentration profiles. Contrib Mineral Petrol 157:163–172

Watson EB (1981) Diffusion in magmas at depth in the Earth; the effects of pressure and dissolved H_2O. Earth Planet Sci Lett 52:291–301

Zhang Y, Ni H, Chen Y (2010) Diffusion data in silicate melts. Rev Mineral Geochem 72:311–408